Center for Turbulence Research
Proceedings of the Summer Program 1994

Anisotropic structure of homogeneous turbulence subjected to uniform rotation

By C. Cambon[1], N. N. Mansour[2] AND K. D. Squires[3]

Large-eddy simulation results are used to investigate the development of anisotropies and the possible transition towards a quasi two-dimensional state in rotating turbulence at high Reynolds number. The present study demonstrates the existence of two transitions that are identified by two Rossby numbers. The first transition marks the onset of anisotropic effects and corresponds to a macro Rossby number Ro^L (based on a longitudinal integral length scale) near unity. A second transition can be defined in terms of a lower bound of a micro-Rossby number Ro^ω also near unity (defined in this work as the ratio of the rms fluctuating vorticity to background vorticity) and corresponds to a continued development of anisotropy but with an increasing emergence of those indicators based on the pure two-dimensional component of the flow, e.g., integral length scales measured along the rotation axis. Investigation of the vorticity structure shows that the second transition is also characterized by an increasing tendency for alignment between the fluctuating vorticity vector and the basic angular velocity vector with a preference for corrotative vorticity.

1. Introduction

Turbulence plays an important role in the performance of many engineering systems where the mean flow is dominated by rotation, technologically relevant examples include the flow in turbomachines as well as reciprocating engines with swirl and tumble. The difficulty in evaluating the performance of these systems is due primarily to their complex nature and to the poor performance of turbulence models used for prediction of the flow fields encountered in these systems. The principal reason for deficiencies in turbulence modeling of rotating flows is in turn related to the fact that mean rotation has an indirect and subtle effect on quantities such as the turbulence kinetic energy and its dissipation rate, i.e., mean rotation does not appear explicitly in the transport equations for either quantity. However, accounting for system rotation is crucial since it alters the nonlinear interactions among turbulent scales. Thus, a better understanding of the effects of system rotation on turbulent flows is needed to properly guide the development of turbulence models.

A flow particularly well suited for increasing our fundamental understanding is rotating homogeneous turbulence since the effect of system rotation can be examined

1 Ecole Centrale de Lyon, France
3 NASA-Ames Research Center
3 The University of Vermont

independent of other complicating influences such as mean gradients, body forces (other than the Coriolis force), wall effects, or organized structures. A topic central to studies of rotating homogeneous turbulence is the generation of anisotropy by background rotation and possible transition towards a quasi two-dimensional state. Important in this regard is that it can be shown that the initial breaking of isotropy arises ultimately from nonlinear interactions which are modified by system rotation (Cambon & Jacquin 1989). Thus, the range of Reynolds and Rossby numbers for which anisotropy will develop is not easily predicted. Furthermore, the typical measures used to describe anisotropy, e.g., that of the Reynolds stress and length scales, require a detailed two-point approach which should also include angular dependence of the distribution of the energy density in wave space. It is also important to emphasize that the Taylor-Proudman theorem cannot predict a transition from a three-dimensional to a two-dimensional structure at zero Rossby number, but only shows that the 'slow manifold' (i.e., the manifold which is unaffected by the linear 'rapid' effects of rotation or inertial waves) is the 'two-dimensional manifold' (see Proudman 1916, Cambon, Mansour & Godeferd 1994).

Insight into the development of anisotropic features in rotating turbulence was examined using direct numerical simulation (DNS) and large-eddy simulation (LES) by Bardina, Ferziger & Rogallo (1984). They found that anisotropy is primarily reflected by the integral length scales whereas the Reynolds stress tensor remained quasi-spherical. Bardina *et al.* did not address, however, the underlying anisotropic spectral shape nor the relevant parameter regime for anisotropy development. Several investigators have used both theoretical and experimental approaches (Jacquin, Leuchter & Geoffroy 1989, Cambon & Jacquin 1989, and Jacquin, Leuchter, Cambon & Mathieu 1990) to investigate anisotropic effects in rotating turbulence, including a non-isotropic spectral description by Cambon (1982) which provided further insight into characterizing the key anisotropy indicators and the relevant parameter ranges over which anisotropic effects would develop. These studies showed that the most important indicators are expressed using the integral length scales with vertical (along the basic rotation axis) separation and vertical or horizontal velocity components. These previous works also support the conjecture that anisotropy in rotating turbulence is triggered when a macro-Rossby number Ro^L becomes smaller than unity. An optimal collapse of measurements was obtained by defining Ro^L as

$$Ro^L = \frac{\sqrt{\langle u_3^2 \rangle}}{2\Omega_3 L_{33}^3} \tag{1}$$

where Ω_3 is the angular velocity of the rotating frame (without loss of generality we choose the vertical direction x_3 along the rotation vector and in what follows we shall drop the subscript from the definition, i.e., $\Omega = \Omega_3$), u_i is the velocity fluctuation, and $\langle\rangle$ denotes statistical averaging. The integral length scales are defined using the two-point correlation

$$L_{ij}^n = \frac{\int_0^\infty \langle u_i(\mathbf{x},t) u_j(\mathbf{x}+r\mathbf{n},t)\rangle dr}{\langle u_i(\mathbf{x},t) u_j(\mathbf{x},t)\rangle} \tag{2}$$

where no summation is implied in the above definition and **n** is the unit vector in the direction referred to by the superscript n.

Evidence of a second transition in the development of anisotropic features in rotating turbulence has come mainly from computational approaches, both DNS as well as EDQNM, where high rotation rates are more easily attained than in laboratory experiments (e.g., see Mansour, Cambon & Speziale 1991a,b). The second transition corresponds to the lower limit of an intermediate range of Rossby numbers in which nonlinear, and therefore the non-isotropic, effects of rotation are statistically insignificant. It is conjectured that the second transition occurs when a micro-Rossby number $Ro^\lambda \sim u'/(2\Omega\lambda)$ (based on a Taylor microscale λ) is smaller than 1. For $Ro^\lambda < 1$ non-linear interactions are negligible, e.g., nearly zero derivative skewness, and the flow can be accurately predicted using Rapid Distortion Theory (RDT). It is important to point out that the RDT solution cannot lead to the development of anisotropy, e.g., Speziale *et al.* (1987) have shown that starting with an initially isotropic flow, the flow remains isotropic under very rapid rotation. Mansour *et al.* (1991c) have shown that while rotation will change the anisotropy of the Reynolds stress tensor due to the scrambling effects of rotation, it does not lead to the generation of new anisotropy. It should also be pointed out that one can predict a reduction of the dimensionality, which is part of the anisotropy development (Cambon & Jacquin 1989), of rotating turbulence by consideration of resonant triads selected at very low Rossby number (Waleffe 1991). However, it is not possible to predict the range of Rossby numbers over which the reduction may occur nor the measure of the manifold of resonant triads relative to all possible triads using this approach. Since the Taylor microscale can be defined from different components in anisotropic turbulence, similar to the integral length scales, it is more convenient to mark the second transition using a micro-Rossby number defined in terms of the vorticity

$$Ro^\omega = \frac{\sqrt{\langle \omega_i \omega_i \rangle}}{2\Omega} \tag{3}$$

where $\omega_i = \epsilon_{ijk} u_{k,j}$. Note that Ro^λ and Ro^ω are proportional since $\omega' \sim u'/\lambda$.

Based upon the summary presented above, there exists evidence to support the simple scheme of an intermediate range of Rossby numbers over which anisotropies in rotating turbulence will develop. This range is marked by a macro-Rossby number close to 1 (where the macro-Rossby number is based on "vertical" quantities) for the upper bound and a micro-Rossby close to 1 for the lower bound. The intermediate range of Rossby numbers involves the Reynolds number through the ratio L/λ and is also consistent with the classical use of an 'Oszmidov scale' (Jacquin *et al.* 1989). The Oszmidov scale for rotation can be defined by $Lo = (\epsilon/(2\Omega)^3)^{1/2}$ (see also Zeman 1994) where the Brunt-Wäisälä frequency has been replaced by the basic vorticity 2Ω so that Lo characterizes the smallest scale up to which the rotation is acting. A value of the macro-Rossby number nearly 1 corresponds to an Oszmidov scale close to the integral length scale $Lo = L$, whereas the micro-Rossby number close to unity corresponds to an Oszmidov scale near the Kolmogorov scale $Lo = \eta$. Hence, the intermediate range of Rossby numbers can be linked to the

largest ($L \sim k^{3/2}/\epsilon$) and the smallest length scales ($\eta = (\nu^3/\epsilon)^{1/4}$) having physical relevance in homogeneous turbulence.

While the majority of previous work has provided evidence of two transitions in the development of anisotropy in rotating turbulence, there exists no previous work in which *both* transitions are evident in the same experimental case or computational run. It is difficult in experiments to obtain large enough rotation rates to observe the second transition while previous computations have not had statistical samples large enough to observe the first transition. An additional difficulty associated with DNS is that the Reynolds number range achievable in DNS prohibits a detailed examination of the generation of anisotropy arising from non-linear interactions since molecular viscosity effectively drives the flow to the RDT limit before non-linear effects become significant. Thus, the most viable approach for examining anisotropy development is simulations performed at high Reynolds numbers using large-eddy simulation. Relevant in this regard is the recent LES study by Bartello, Métais and Lesieur (1994). Bartello *et al.* examined the structural evolution of initially isotropic turbulence subjected to uniform system rotation and observed a single transition marking the generation of anisotropy. The transition in their work occurred around $Ro^\omega \sim 1$ (referred to as the second transition above) with significant anisotropy developing only for $Ro^\omega < 1$.

Therefore, the primary motivation of the work presented in this paper has been to provide a detailed examination of the evolution of statistical and structural anisotropy indicators in rotating homogeneous turbulence at high Reynolds numbers. Especially important to this work are simulations of rotating homogeneous flows in which the intermediate range of Rossby numbers is achieved, i.e., $Ro^L < 1$ and $Ro^\omega > 1$ in order to permit observation of all possible transitions. Of further interest in this work is examination of the underlying structure of the vorticity field as anisotropy develops. Evidence exists of a tendency for alignment of the vorticity along the rotation axis with a preference for alignment of corrotative (i.e., parallel or cyclonic) vorticity compared to contrarotative (i.e., antiparallel or anticyclonic) vortices (e.g., see Bartello *et al.* 1994).

An overview of the LES database used in this work is presented in §2, including time development of measures of the anisotropy and examination of the vorticity structure using a joint pdf of the cosine of the angle between the x_3-component of the vorticity vector and background rotation vector with the local micro-Rossby number $\omega_i\omega_i/(2\Omega)$. Discussed in §3 is the anisotropy 'shape', i.e., interpretation of the 'cigar type' of covariance matrices for both the velocity and the vorticity field, using extensively the concepts of 'directional dependence' and 'polarization' (Cambon, Jacquin & Lubrano 1992) or, almost equivalently, those of 'dimensionality' and 'componentality' (Reynolds & Kassinos 1994). The relevance of a classic centrifugal instability for predicting the asymmetry of the vorticity structure in terms of corrotative and contrarotative vortices is discussed, together with a summary of the work from this study, in §4.

2. Database overview and simulation results

2.1. LES database

In this work a pseudo-spectral method was used to integrate the filtered Navier-Stokes equations for an incompressible fluid in a rotating reference frame. The formulation uses an implicit treatment of linear rotation terms which allows exact integration of the rapid distortion equations (Rogallo 1981, Mansour *et al.* 1991a). Subgrid-scale stresses were parameterized using a spectral-eddy viscosity (Kraichnan 1976, Chollet & Lesieur 1981) modified for rotating turbulence (see Cambon, Bertoglio & Jeandel 1981 and Squires, Chasnov, Mansour & Cambon 1994). Use of a subgrid-scale model yields a third relevant Rossby number

$$Ro^{sg} = \sqrt{\frac{E(k_c,t)k_c^3}{8\Omega^2}} \tag{4}$$

referred to as the cut-off Rossby in this manuscript (k_c is the cut-off wavenumber and $E(k,t)$ the classic shell-averaged energy spectrum). Since the molecular viscosity was dropped from the Navier-Stokes equations, the simulations can be considered to represent asymptotically the dynamics at infinite Reynolds number.

The computations were performed using an elongated domain in which the vertical dimension is four times the horizontal length. This geometry and the isotropic initial data were carefully optimized in order to permit the development of the flow without disturbing statistical symmetries. This is especially important in the present work since the initial three-dimensional isotropy is broken only by nonlinear dynamics. Care was also exercised in order to insure that the length scales remain small compared to the size of the computational box. Four datasets were used in the course of this work: the first case (referred to as D0) was obtained at a resolution of $64 \times 64 \times 256$ collocation points and rotation rate of 0.1. Case D0 was used primarily as a means of obtaining preliminary structural results but also permits examination of the effect of resolution. The other cases, referred to as D1, D2, and D3 for computations performed using rotation rates of 0.1, 0.5, and 1.0, respectively, were performed using resolutions of $128 \times 128 \times 512$ collocation points. The reader is referred to Squires, Chasnov, Mansour & Cambon (1993, 1994) for additional details concerning the simulations.

2.2. Statistical evolution

Shown in Fig. 1 are the time histories of the three relevant Rossby numbers Ro^L, Ro^ω, and Ro^{sg} for Cases D0 and D1 (Fig. 1*a*), Case D2 (Fig. 1*b*), and Case D3 (Fig 1*c*). The time axis in Fig. 1 has been made dimensionless by the initial eddy turnover time. It is evident from the figure, especially for Cases D0 and D1, that the initial value of any Rossby number is large enough to ensure that the rotation has an initially weak influence and that there is adequate time for development of triple correlations as in non-rotating turbulence. We find that as in previous DNS and experimental studies, the value of the macro- and the micro-Rossby numbers decrease with time. Eventually, the intermediate range of Rossby numbers, i.e.,

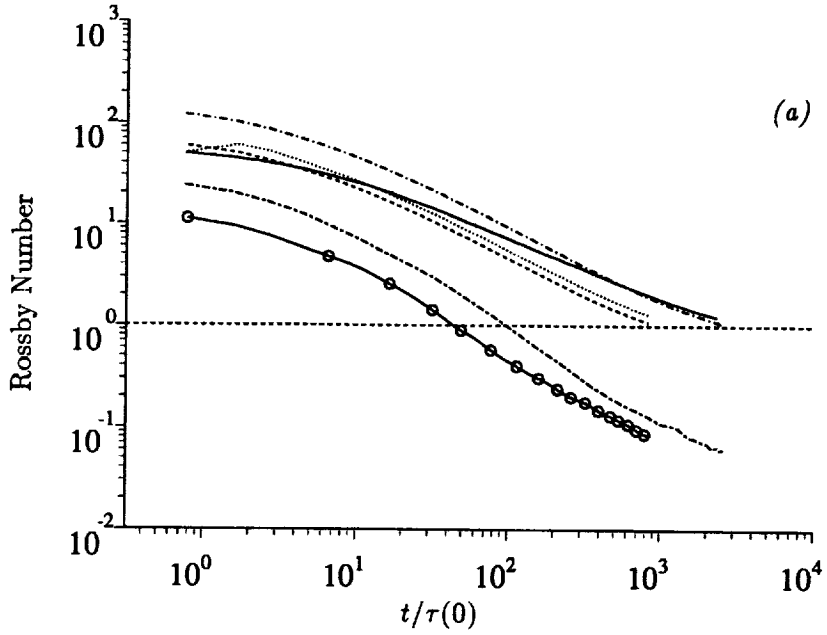

FIGURE 1A. Rossby number development. (*a*) Case D0: ⟜⟜ Ro^L; ---- Ro^ω; ····· Ro^{sg}. Case D1: —·— Ro^L; —·— Ro^ω; —— Ro^{sg}.

$Ro^L < 1$ and $Ro^\omega > 1$, is attained during the simulation. Fig. 1*a* shows that the intermediate range is maintained for more than a decade for Case D1, ending at approximately the final time of the calculation. In addition, the results in Fig. 1 also show the effect of resolution (Cases D0 and D1) as well as a portion of the calculation occurring after the second transition (Cases D2 and D3).

To test the validity of computing statistics using only the large scales in an LES computation, Chasnov (1994) assumed that an inertial range extends towards infinity after the cut-off wavenumber. Chasnov found that this extension of the spectrum yields relatively small corrections to the values of the kinetic energy and the integral length scales as compared to computing these values from the resolved scales. Thus, computing the macro-Rossby number using data from only the resolved scales does not present any theoretical or practical difficulties. Because the smallest scales of motion are not represented in large-eddy simulation, however, the definition of a micro-Rossby deserves additional discussion. It is worth noting that an extension of the spectrum past the cut-off wavenumber to account for the unresolved scales will result in a divergent vorticity field; therefore, this approach cannot be used to define a micro-Rossby number. Thus, in this work the micro-Rossby number shall be defined using the vorticity field from the resolved scales, yielding an effective Ro^ω in the same way as the use of an eddy viscosity in LES yields an effective Reynolds number.

Note that it is also possible to define a pseudo-Reynolds number Re^* based on the resolved scales as the ratio between the macro- and the micro-Rossby numbers in

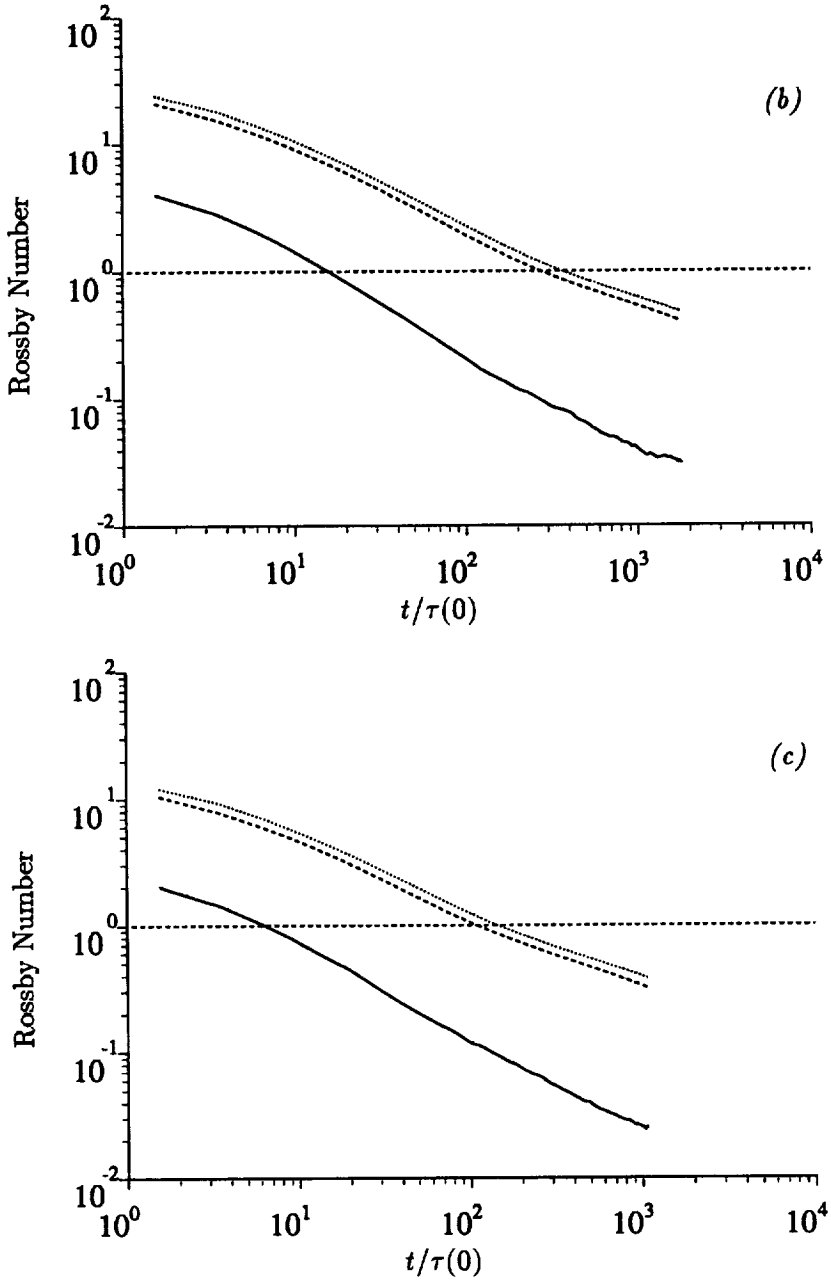

FIGURE 1B - C. Rossby number development. Case D2 (*b*) and Case D3 (*c*): —— Ro^L; ---- Ro^ω; ····· Ro^{sg}.

agreement with the isotropic relationship, i.e., $Re^* = k^2/(\nu\epsilon) = (2/3)(Ro^\omega/Ro^L)^2$. The time development of Re^* is presented in Fig. 2. As opposed to the behavior observed in DNS and experiments, Re^* increases with elapsed time since the integral

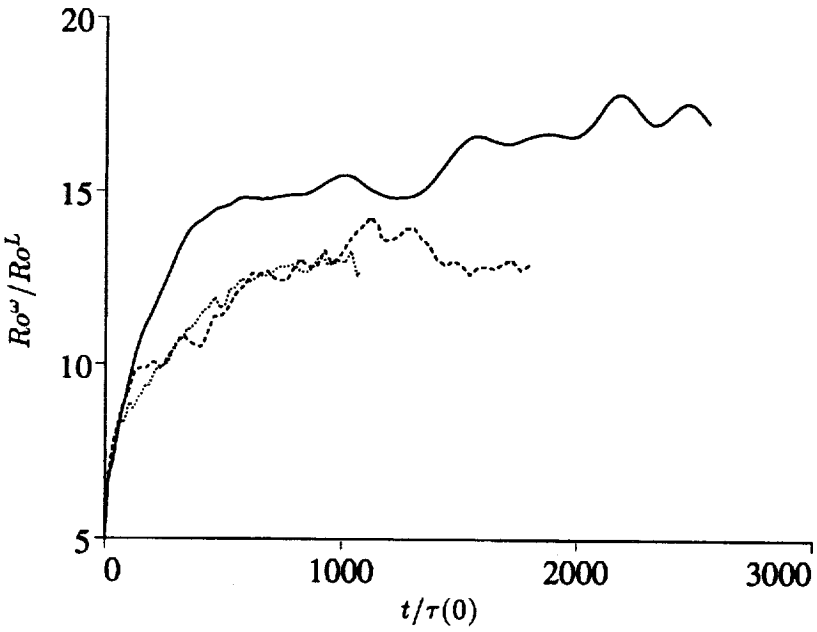

FIGURE 2. Time development of "Reynolds number". —— Case D1; ---- Case D2; ····· Case D3.

length scale continually increases while the resolved Taylor microscale (or $\lambda \propto u'/\omega'$) tends to be blocked by the cut-off scale $2\pi/k_c$. The latter behavior is consistent with the nearly equivalent values of Ro^ω and Ro^{sg}, with the exception of very early times in the development (Fig. 1). Some discrepancies between Cases D0 and D1 shown in Fig. 1*a* illustrate the effect of the resolution: Ro^ω and Ro^{sg} are shown to be nearly equal during the entire time development only at the finer resolutions.

Of the various statistical measures of anisotropy, the measure most widely utilized in previous investigations has been that of the Reynolds stress, i.e., $b_{ij} = R_{ij}/R_{ll} - \delta_{ij}/3$, where $R_{ij} = \langle u_i u_j \rangle$. Note that there is only one component relevant in the semi-axisymmetric configuration created by rotation, $b_{33} = b_{ij}\frac{\Omega_i\Omega_j}{\Omega^2}$, since $b_{11} = b_{22} = -b_{33}/2$ and the off-diagonal components are zero. Fig. 3 shows the evolution of the Reynolds stress anisotropy as a function of time for the three high resolution cases considered. We find a mild positive maximum value of about 0.06 which is consistent with a 'cigar-type' shape (i.e., elongation in one direction) for the Reynolds stress tensor with a ratio of horizontal and vertical principal components $\frac{1}{2}(\langle u_1^2\rangle + \langle u_2^2\rangle)/\langle u_3^2\rangle$ about 0.7-0.8. A very good collapse of the 3 cases (D1, D2, D3) is demonstrated in Fig. 4 in terms of the macro-Rossby number and the anisotropy does indeed appear to be triggered around $Ro^L = 1$. A similar collapse, and further confirmation of the first transition, is found using the vorticity ratio $\frac{1}{2}(\langle \omega_1^2\rangle + \langle \omega_2^2\rangle)/\langle \omega_3^2\rangle$. In order to provide an anisotropy measure for the vorticity in agreement with the one used for the velocity, the component b_{33}^ω of the vorticity

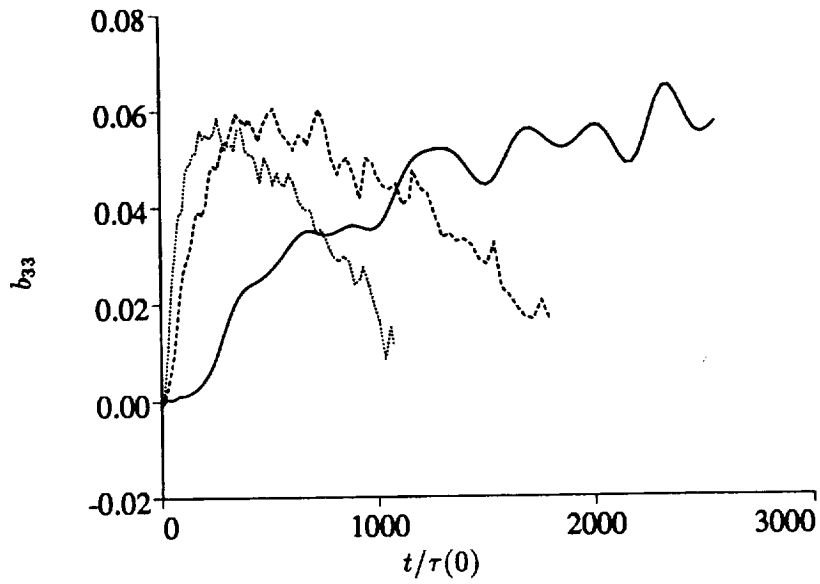

FIGURE 3. Time development of b_{33} component of Reynolds stress anisotropy. —— Case D1; ---- Case D2; ····· Case D3.

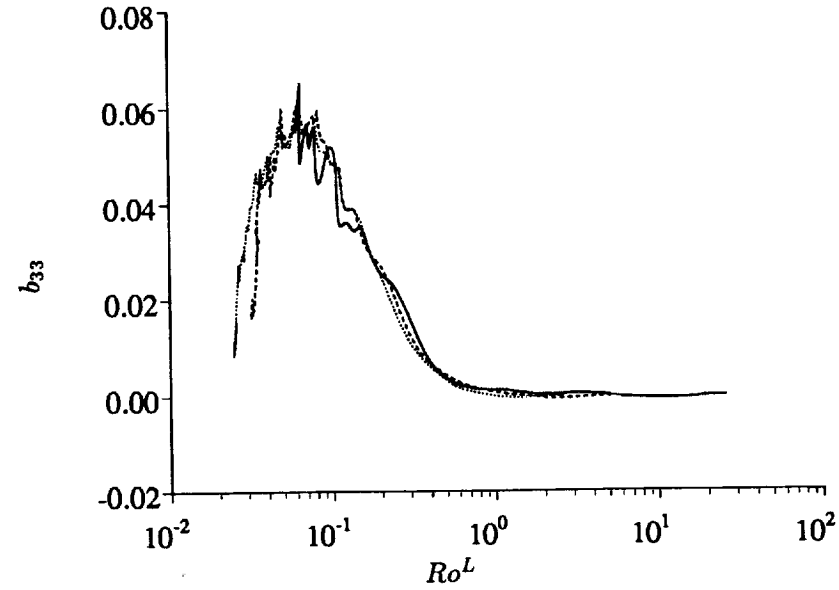

FIGURE 4. Development of b_{33} as a function of the macro Rossby number. —— Case D1; ---- Case D2; ····· Case D3.

deviator

$$b^{\omega}_{ij}\frac{\Omega_i\Omega_j}{\Omega^2} = b^{\omega}_{33} = \frac{\langle\omega_3^2\rangle}{\langle\omega^2\rangle} - \frac{1}{3} \tag{5}$$

is plotted in Fig. 5. We find that the vorticity tensor exhibits the same type of anisotropy shape ('cigar-type') as the Reynolds stress tensor.

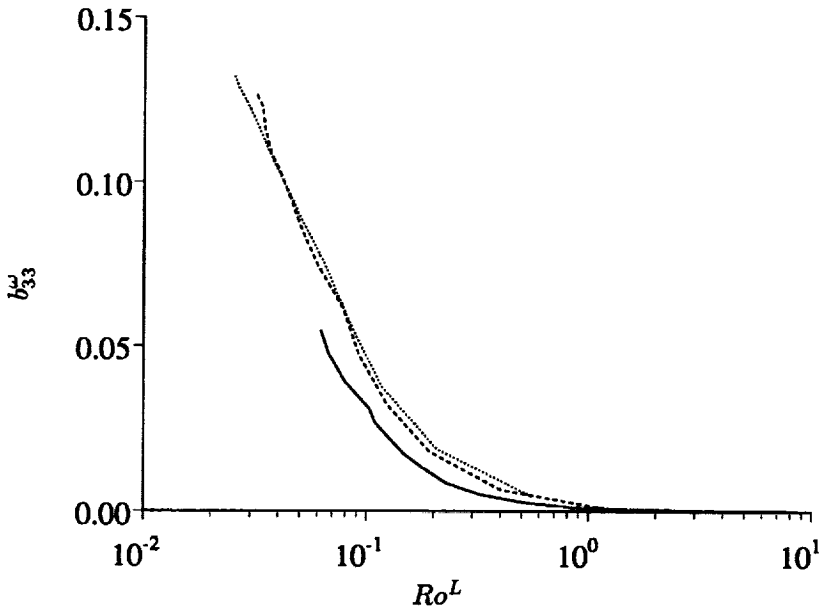

FIGURE 5. Development of vorticity anisotropy b^{ω}_{33} as a function of the macro Rossby number. —— Case D1; ---- Case D2; ····· Case D3.

Similar anisotropy is also found using the most relevant integral length scales, L^3_{33} and $L^3_{11} + L^3_{22} = 2L^3_{11}$ (Fig. 6). An anisotropy measure of the integral length scales can be defined as

$$b^L = \frac{\langle u_1^2 \rangle L^3_{11} + \langle u_2^2 \rangle L^3_{22}}{\sum_{i=1,3} \langle u_i^2 \rangle L^3_{ii}} - \frac{1}{2} \tag{6}$$

based on a true tensor of '2D-energy components' $\mathcal{E}^3_{ij} = \langle u_i u_j \rangle L^3_{ij}$ (Cambon 1990). The quantity b^L is shown in Fig. 7 and is also consistent with the results observed in Figs. 4-6.

Finally, it is interesting to note that the slight plateau exhibited in Fig. 3 and Fig. 4 is consistent with the blocking of nonlinear anisotropic effects previously observed in DNS and EDQNM computations after the second transition $Ro^{\omega} \sim 1$. However, the fact that the anisotropy reflected by the vorticity ratio and the integral length scale ratio continues to increase after the second transition ($Ro^{\omega} < 1$) is surprising and requires further investigation.

2.3. *Vorticity structure*

The anisotropy reflected by the Reynolds stress tensor and the vorticity correlation tensor has motivated a refined structural analysis. The joint-probability of $\cos\alpha = \omega_3/\omega$ and of the local Rossby number, $\sqrt{\omega_i \omega_i}/2\Omega$, is plotted for different

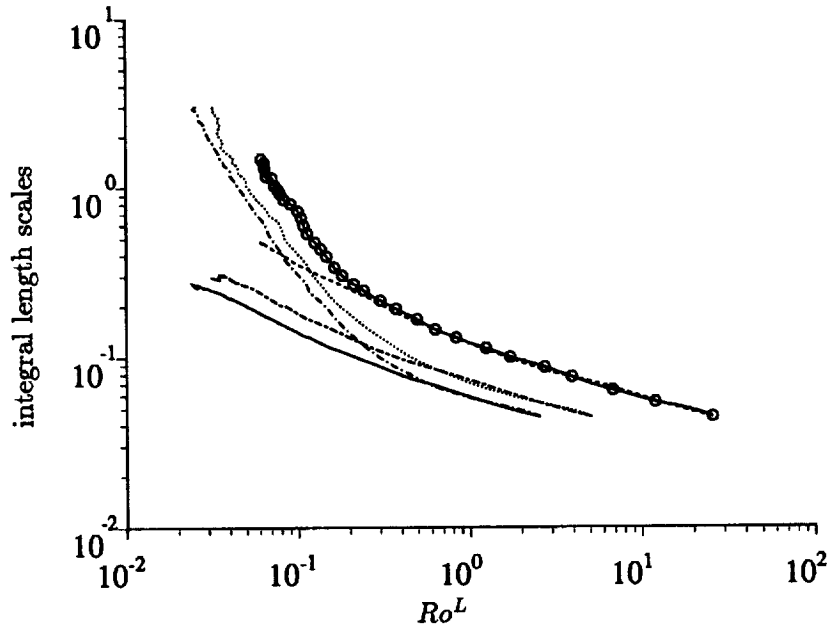

FIGURE 6. Development of integral length scales L_{33}^3 and L_{11}^3 as a function of the macro Rossby number. Case D1: o—o $L_{11}^3 + L_{22}^3$; ---- L_{33}^3. Case D2: ····· $L_{11}^3 + L_{22}^3$; — — L_{33}^3. Case D3: —·— $L_{11}^3 + L_{22}^3$; —— L_{33}^3.

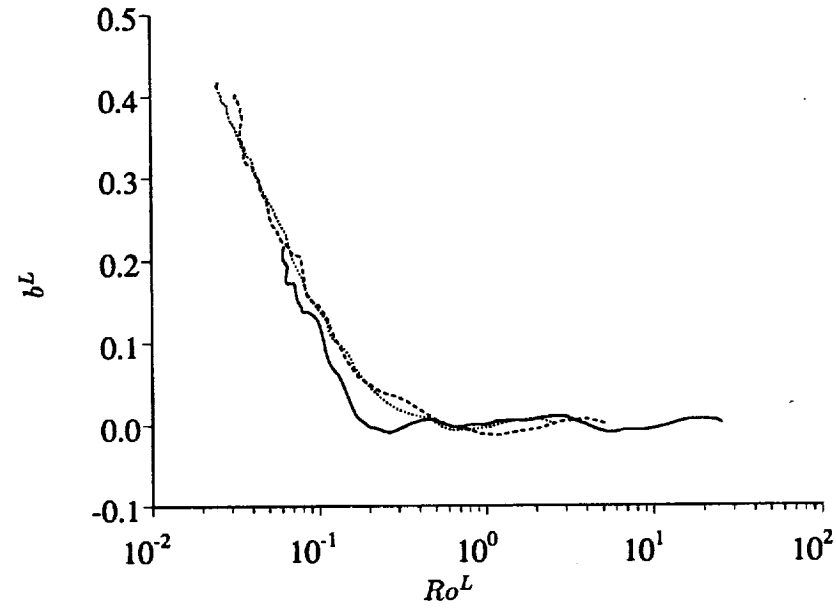

FIGURE 7. Development of length scale anisotropy b^L as a function of the macro Rossby number. —— Case D1; ---- Case D2; ····· Case D3.

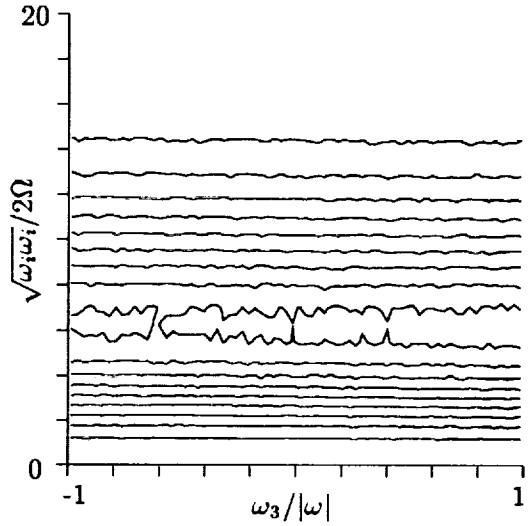

FIGURE 8. Joint pdf of local Rossby number and cosine of the angle between vertical vorticity and vorticity magnitude for Case D2, $t/\tau(0) = 13$. Contour levels drawn between 0 and 8 with an interval of 0.4.

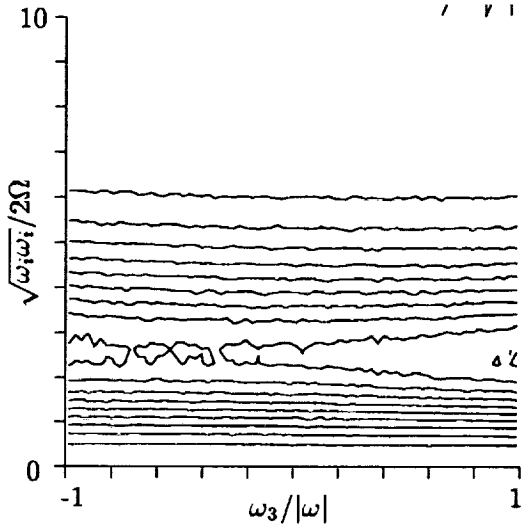

FIGURE 9. Joint pdf of local Rossby number and cosine of the angle between vertical vorticity and vorticity magnitude for Case D2, $t/\tau(0) = 48$. Contour levels drawn between 0 and 8 with an interval of 0.4.

times in Figs. 8 through 11. The x-axis represents binning in terms of the cosine of the angle between the rotation axis and the vorticity vector. Values of the cosine equal to -1 represent contrarotative or antiparallel eddies, values of the cosine equal to 1 represent corrotative or parallel eddies. The use of the cosine of the angle rather than the angle itself ensures equal probability of occurrence in any bin. The

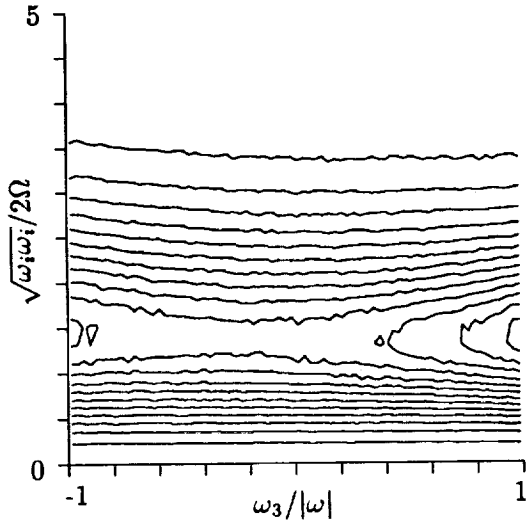

FIGURE 10. Joint pdf of local Rossby number and cosine of the angle between vertical vorticity and vorticity magnitude for Case D2, $t/\tau(0) = 109$. Contour levels drawn between 0 and 8 with an interval of 0.4.

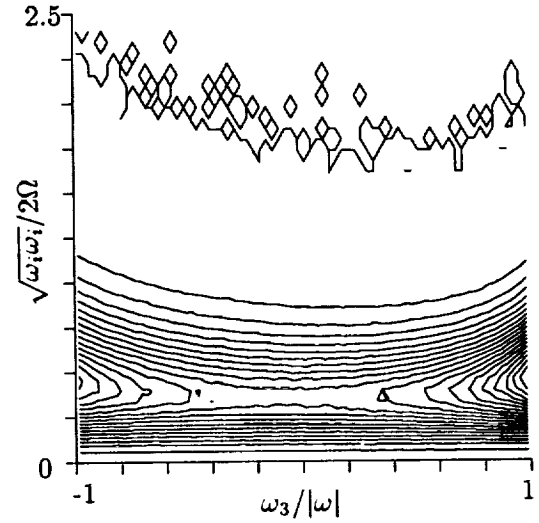

FIGURE 11. Joint pdf of local Rossby number and cosine of the angle between vertical vorticity and vorticity magnitude for Case D2, $t/\tau(0) = 1168$. Contour levels drawn between 0 and 8 with an interval of 0.4.

y-axis represents binning in terms of the local micro-Rossby number, and because Ω is uniform, it is also a measure of the magnitude of the vorticity fluctuation. Fig. 8 corresponds to the beginning of the intermediate range ($Ro^L = 1, Ro^\omega = 8$, see Fig. 1*a*) and the horizontal layering reflects a complete isotropy at a very fine level (statistical equidistribution of the orientation of the vortices). At smaller Ro^ω

ranging from 2 to 1 (Figs. 9 to 11), the distribution shows a distinct tendency for the vortices to be increasingly aligned with the basic rotation axis. The distribution exhibits two peaks near $\cos\alpha = 1$ and $\cos\alpha = -1$ with a preference of corrotative eddies ($\cos\alpha = 1$) clearly exhibited in the distribution. This finding is consistent with that previously observed by Bartello *et al.* (1994) that corotating vorticity tends to become the dominant vorticity in the flow.

3. Interpretation of the anisotropic structure

3.1. Velocity and vorticity fields

The development of anisotropy can be easily argued for most homogeneous flows based upon the type of mean deformation. For instance, the anisotropy created by a distorting duct can be interpreted as follows: in the direction of maximum stretching (chosen as x_3 for sake of discussion), the vorticity is elongated so that the intensity of vortices is reinforced in accordance with conservation of angular momentum and $\langle\omega_3^2\rangle$ becomes dominant with respect to other (horizontal) principal components. In this case the covariance $\langle\omega_i\omega_j\rangle$ assumes a 'cigar type' shape under the influence of the mean strain. Because of the more rapid rotation of the eddy in the plane normal to the axis of stretching, the velocity components orthogonal to the x_3 axis will become larger, creating a 'pancake type' shape for the tensor $\langle u_i u_j\rangle$, i.e., two dominant components relative to a third weak component. The interesting feature of the rotating flow, however, is that *both* the single-point covariance matrices of the velocity and vorticity field possess a 'cigar type' shape. This is a very specific feature not observed in other anisotropic flows subjected to mean deformation and in turn motivates a more refined interpretation than can be obtained from Figs. 3-5.

The specific anisotropy created by rotation through non-linear interactions can best be described using a two-point approach, or at least a single-point approach that carries information about both the 'dimensionality' and 'componentality' of the flow. For this purpose it is convenient to utilize spectral variables (e, Z, h) that completely characterize the double correlations at two points for any homogeneous anisotropic field. These three variables are invariants of the flow: the energy, e, the polarization anisotropy, Z, and the helicity, h, and correspond to double correlations of the two components (or helical modes intensities) in the plane normal to the wave vector $\mathbf{k}$ (see Cambon & Jacquin 1989 for a complete discussion). In the semi-axisymmetric configuration created by rotation through nonlinear effects, only e and Z are relevant and they depend only on the wavevector modulus k and on the cosine of the angle between $\mathbf{k}$ and $\mathbf{\Omega}$, i.e., $\cos\theta_k = k_3/k$. It is important to note that e is a three-dimensional energy spectrum ($e \propto \frac{1}{2}\langle\widehat{u}_i^*\widehat{u}_i\rangle$) but is not spherically averaged. Thus, the difference between e and the spherically averaged value, i.e., $e(k, cos\theta_k) - E(k)/(4\pi k^2)$, characterizes a directional anisotropy. The complex scalar Z gives at fixed $\mathbf{k}$ the difference of the two nonzero principal components of $\langle\widehat{u}_i^*\widehat{u}_j\rangle$ as its modulus, $|Z|$, and the orientation of the related principal axes as its argument. Thus, Z characterizes a polarization anisotropy. The transport of these quantities is governed by

$$\left(\frac{\partial}{\partial t} + 2\nu k^2\right) e(k, k_3/k, t) = T^e(k, k_3/k, t) \qquad (7a)$$

and

$$(\frac{\partial}{\partial t} + 2\nu k^2 + 4i\Omega\frac{k_3}{k})\, Z(k, k_3/k, t) = T^z(k, k_3/k, t) \tag{7b}$$

which describes the dynamics in the presence of rotation with an exact separation of contributions from linear (or rapid) terms on the left hand sides and of contributions from nonlinear terms on the right hand sides. The terms T^e and T^z are spectral transfer terms that involve cubic correlations. In an LES calculation T^e and T^z may be replaced by $(T^e - 2\nu_{sg}k^2 e)$ and $(T^z - 2\nu_{sg}k^2 Z)$, so that ν is replaced by ν_{sg} in (7), whereas $T^{(\cdot)}$ denote the resolved transfer terms.

One of the primary advantages of the decomposition into the invariants e and $|Z|$ is that the spectral tensor of double correlations, vorticity as well as velocity, at two points can be expressed in terms of e and Z in a fixed frame of reference. Any single-point tensor obtained by subsequently integrating in wave-space can then be split into a pure (three-dimensional) isotropic contribution (from $E/(4\pi k^2)$), a contribution from the directional anisotropy ($e - E/(4\pi k^2)$), and a contribution from the polarization anisotropy Z. For convenience this splitting is applied to the Reynolds stress tensor,

$$R_{ij} = q^2\left(\frac{\delta_{ij}}{3} + b^e_{ij} + b^z_{ij}\right) \tag{8}$$

and to the tensors introduced by Reynolds & Kassinos (1994), i.e., the dimensionality structure tensor

$$D_{ij} = q^2\left(\frac{\delta_{ij}}{3} - 2b^e_{ij}\right) \tag{9}$$

and the circulicity tensor

$$F_{ij} = q^2\left(\frac{\delta_{ij}}{3} + b^e_{ij} - b^z_{ij}\right). \tag{10}$$

The superscripts e and z in (8)-(10) denote contributions from $e - E/(4\pi k^2)$ and from Z, respectively. The dimensionality tensor

$$D_{ij} = \left\langle \frac{\partial\psi_k}{\partial x_i}\frac{\partial\psi_k}{\partial x_j}\right\rangle \qquad \text{with} \qquad \nabla^2\psi_i = -\omega_i = -\epsilon_{ijk}\frac{\partial u_k}{\partial x_j} \tag{11a}$$

is equivalently defined by

$$D_{ij} = \int 2\frac{k_i k_j}{k^2} e(\mathbf{k}, t) d^3\mathbf{k} \tag{11b}$$

and displays the directional dependence of the spectral distribution of energy. It is clear from (9) and (11) that 'directional dependence' and 'dimensionality' are similar concepts. Eq. (8), however, shows that the 'componentality' of the Reynolds stress tensor (denoted by its deviatoric part b_{ij}) results from additive contributions from 'dimensionality' (or 'directivity') b^e_{ij} and from 'polarization' b^z_{ij}. The circulicity tensor $F_{ij} = \langle\psi_{i,k}\psi_{j,k}\rangle$ characterizes the contribution from the largest scales to

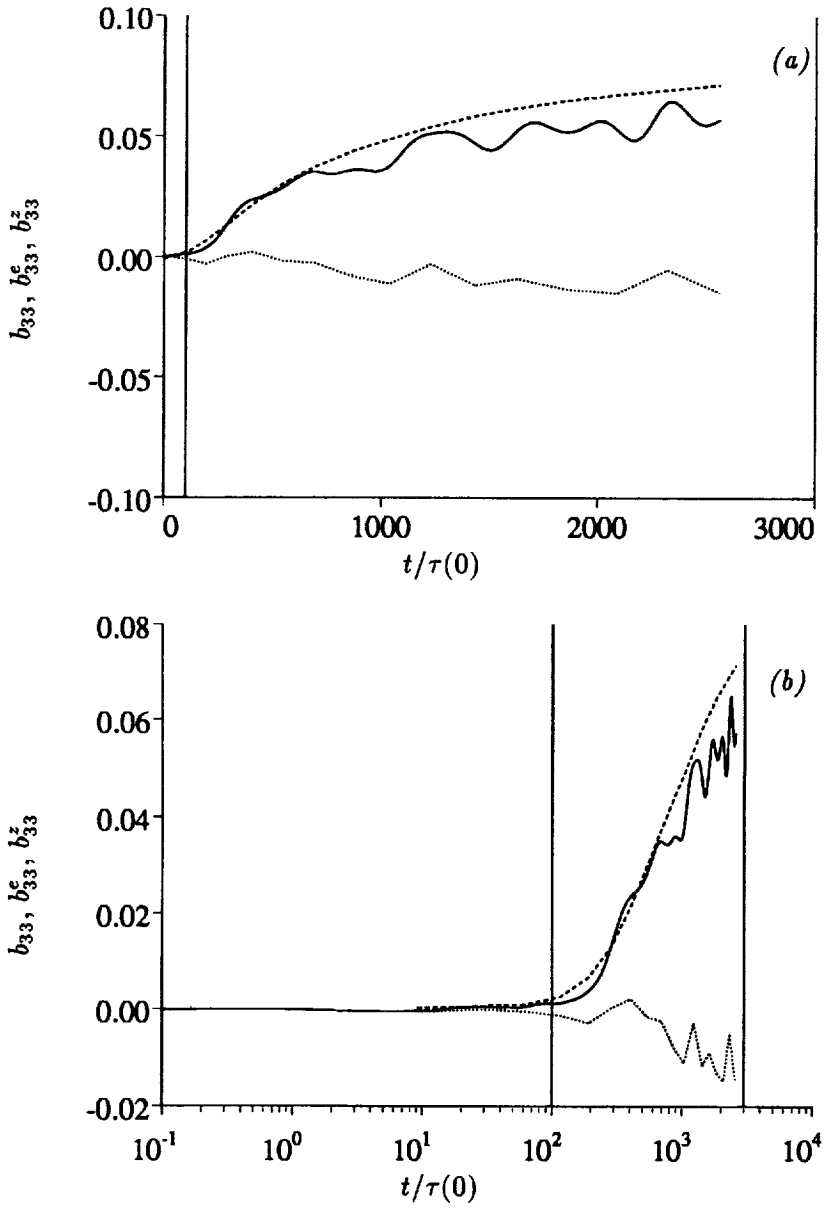

FIGURE 12. Reynolds stress anisotropy for Case D1, intermediate range of Rossby numbers Ro^L and Ro^ω occurring for $100 \leq t/\tau(0) \leq 3000$ (marked by solid vertical lines on figure). —— b_{33}; ---- b_{33}^e; ····· b_{33}^z.

the vorticity covariance matrix since it is obtained by integrating $\langle \widehat{\omega}_i^* \widehat{\omega}_j \rangle / k^2$ (see Eq. 11a). It is also worth noting that the 'directional dependence' of F_{ij} is exactly the same as that of the Reynolds stress tensor whereas its 'polarization' is exactly the opposite.

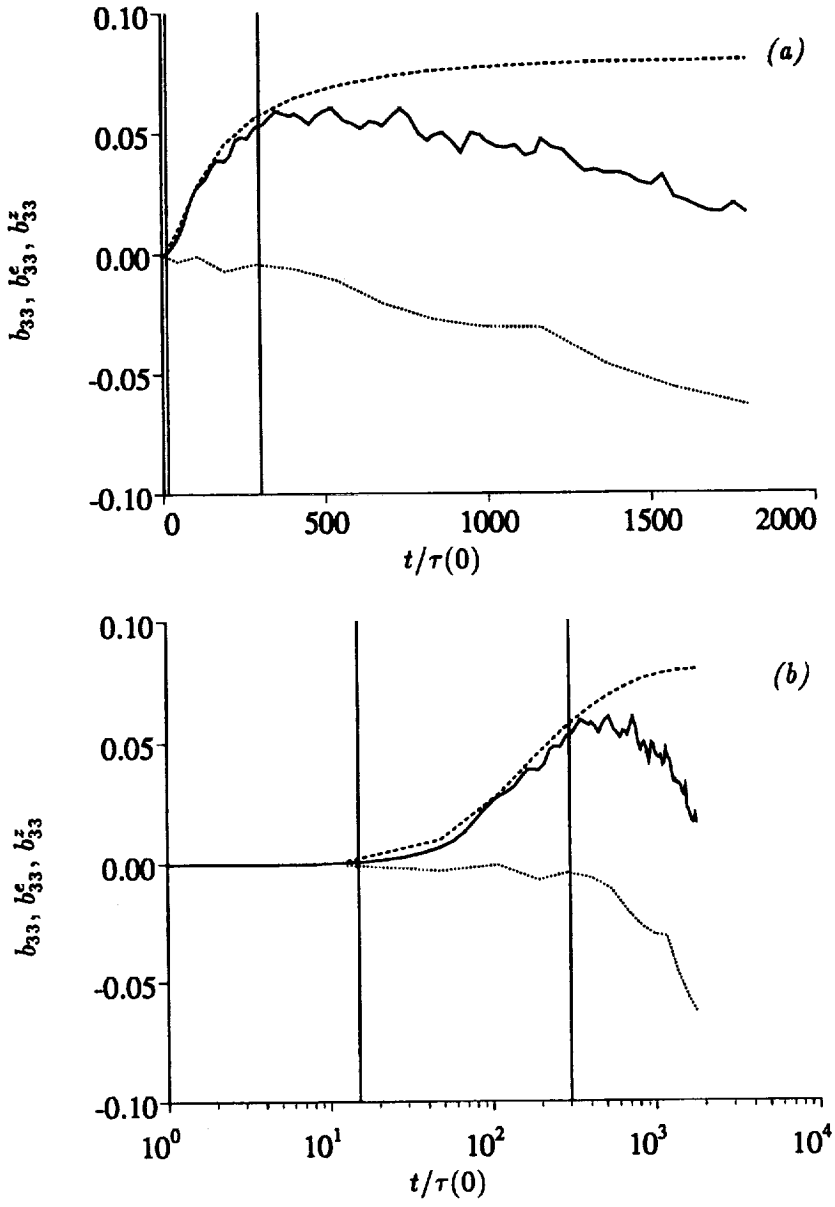

FIGURE 13. Reynolds stress anisotropy for Case D2, intermediate range of Rossby numbers Ro^L and Ro^ω occurring for $15 \leq t/\tau(0) \leq 300$ (marked by solid vertical lines on figure). —— b_{33}; ---- b^e_{33}; ····· b^z_{33}.

Shown in Fig. 12*a* (linear time axis) and Fig. 12*b* (logarithmic time axis) are the relevant anisotropy indicators in semi-axisymmetric turbulence, i.e., b_{33} and components b^e_{33} and b^z_{33}, computed using (8), (9), and (11*b*) for Case D1. The

strong dominance of b_{33}^e relative to b_{33}^z demonstrates that the 'slow' effect of rotation is mainly a 'dimensional' one. This is further supported by the observation that the spectral density of energy tends to concentrate in the wave-plane $k_3 = 0$, i.e., the pure two-dimensional manifold, since a complete concentration at $k_3 = 0$ corresponds to a vanishing of vertical variability in physical space (see Squires *et al.* 1993). If a pure two-dimensional/three-component (2D-3C) state was reached, D_{33}/q^2 would be zero according to (11) so that $b_{33} \sim b_{33}^e$ would be equal to 1/6.

It is also important to remark that the contribution from the 'polarization' indicated by a slightly negative value for b_{33}^z in Fig. 12 is not insignificant. For example, the RDT solution, through scrambling effects by inertial waves, modifies the angle of polarization through a (k_3/k)-dependent angle of rotation $(2\Omega t k_3/k)$ so that the contribution from Z is 'killed off' on average by linear effects and, hence, $b_{33}^z \sim 0$. However, inertial waves cannot affect Z in the slow manifold $k_3 = 0$ where Z is real and the polarization discriminates contributions to vertical velocity components $e + Z$ from contributions to horizontal velocity components $e - Z$. The quantity $e - Z$ at $k_3 = 0$ is precisely the two-dimensional/two-component mode since it contributes only to the horizontal velocity field in the slow (two-dimensional) manifold and $k^2(e - Z)$ contributes only to the vertical vorticity component. Accordingly $e + Z$ at $k_3 = 0$ is the 2D-3C mode in the slow manifold, which only contributes to the vertical velocity component, whereas $k^2(e + Z)$ contributes only to horizontal vorticity components. The dynamics of these two modes of the slow manifold are accounted for in physical space through products of integral length scales and related Reynolds stress components (e.g., Eq. 6) but are weakly reflected by single-point velocity or vorticity correlations obtained by averaging over all angles in spectral space. In any case, examination of contributions from only the slow manifold would indicate that the weak negative value of b_{33}^z may characterize a tendency of the velocity field to be rather horizontal and of the vorticity field to be rather vertical. For the vorticity correlations the 'cigar type' shape created by the 'dimensionality' for the circulicity tensor is slightly increased by polarization (since $b_{33}^e - b_{33}^z > b_{33}^e$) according to (9), whereas the 'cigar type' shape of the Reynolds stress tensor is slightly diminished since $b_{33}^e + b_{33}^z < b_{33}^e$. However, it is important to also note that the 'dimensionality effect' is not balanced by the 'polarization effect'. In addition, the latter effect can be interpreted as a 'componentality effect' but restricted to the slow manifold where inertial waves cannot destroy it.

It is further interesting to examine b_{33} and its contributions from e and Z for Cases D2 and D3. The development shown in Figs. 13 and 14 are consistent with the previous discussion for Fig. 12 but also clearly suggest that the only significant contribution from Z is obtained *after* the second transition in accordance with the location of $Ro^\omega = 1$ (cf. Fig. 1*b* and Fig. 1*c*). The stabilization of b_{33} at early times following the second transition is due to the balanced increase of b_{33}^e and decrease b_{33}^z. For increasing time past the second transition it is also clear from Figs. 13 and 14 that the behavior of b_{33} is driven by the increasingly negative value of b_{33}^z. It is possible that for longer evolution times b_{33} may become negative, indicating a two-dimensional/two-component state of the Reynolds stress tensor. However, it is

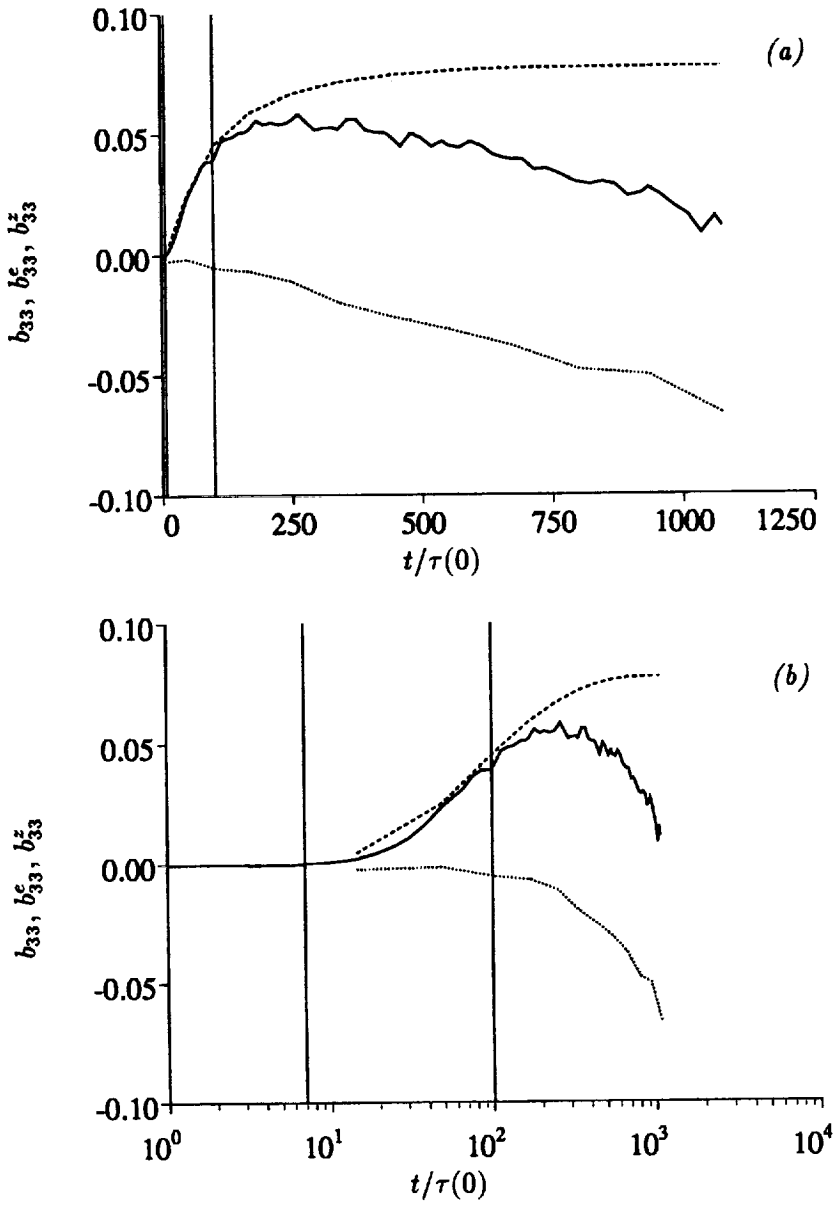

FIGURE 14. Reynolds stress anisotropy for Case D3, intermediate range of Rossby numbers Ro^L and Ro^ω occurring for $7 \leq t/\tau(0) \leq 100$ (marked by solid vertical lines on figure). —— b_{33}; ---- b_{33}^e; ····· b_{33}^z.

difficult to confirm this tendency even in high resolution LES since the imposition of periodic boundary conditions will have an adverse effect on the overall evolution of the flow.

Finally, the three cases are plotted in Fig. 15 in terms of Ro^L. The collapse of the

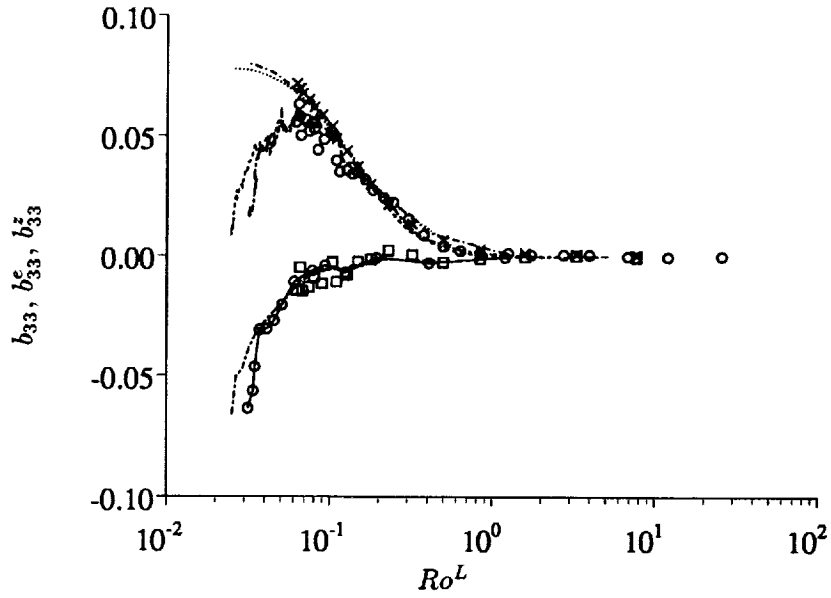

FIGURE 15. Reynolds stress anisotropy as a function of the macro Rossby number. Case D1: ○ b_{33}; × b^e_{33}; □ b^z_{33}. Case D2: —·— b_{33}; —·— b^e_{33}; ○—○ b^z_{33}. Case D3: - - - - b_{33}; ····· b^e_{33}; — — — b^z_{33}.

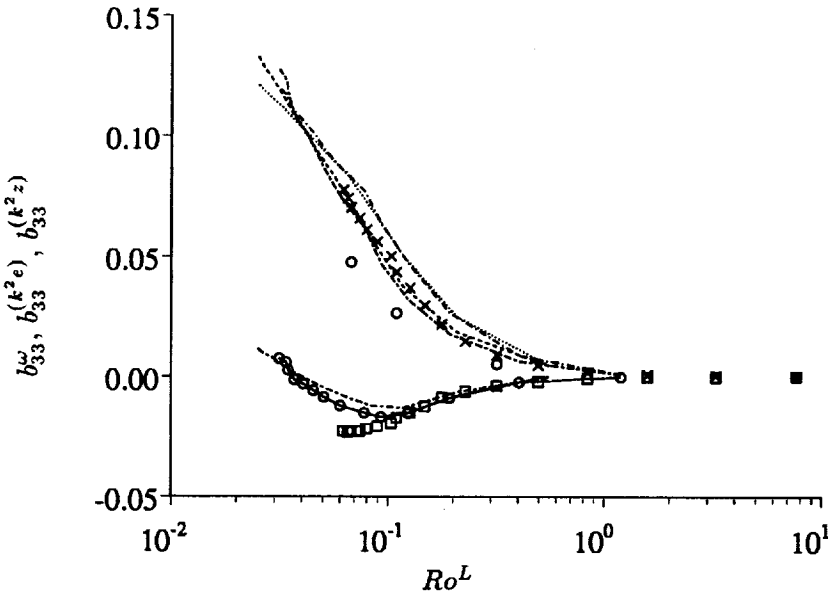

FIGURE 16. Vorticity anisotropy as a function of the macro Rossby number. Case D1: ○ b^{ω}_{33}; × $b^{(k^2e)}_{33}$; □ $b^{(k^2z)}_{33}$. Case D2: —·— b^{ω}_{33}; —·— $b^{(k^2e)}_{33}$; ○—○ $b^{(k^2z)}_{33}$. Case D3: - - - - b^{ω}_{33}; ····· $b^{(k^2e)}_{33}$; — — — $b^{(k^2z)}_{33}$.

data for the three cases is remarkable and demonstrates that the findings discussed for Case D1 apply to the other two cases as well. Furthermore, the results in Fig. 15 also show that the macro Rossby number is the key parameter determining the state of the turbulence. The onset of anisotropy is clearly indicated for $Ro^L < 1$ while a second transition occurs at approximately $Ro^L < 0.1$ which corresponds to $Ro^\omega < 1$.

Analogous quantities to the anisotropy measures of the velocity field shown in Fig. 15 have been plotted in Fig. 16 for the vorticity field. These quantities were calculated using a k^2 weighting factor so that $b_{33}^{(k^2 e)} - b_{33}^{(k^2 z)}$ yields b_{33}^{ω}, i.e., the anisotropy of the single-point vorticity correlation tensor. The relative role of Z (or polarization) in the development of the anisotropy is weak compared to the contribution due to the role of e (i.e., dimensionality). This is a reflection of the concentration of energy around $k_3 = 0$. As was also observed for the velocity, the collapse of the vorticity anisotropy for the three cases in terms of the macro Rossby number is again remarkable. In this case the first transition is clear while the second is marked by a change in the slope of $b_{33}^{(k^2 z)}$.

Finally, it is again worth noting that the 'cigar-type' shape created by the pure 'dimensionality' effect ($b_{33}^{e} > 0$, $b_{33}^{(k^2 e)} > 0$), has nothing to do with a tendency of the velocity vector or the vorticity vector to be aligned with the rotation vector. The relative concentration of spectral energy at $k_3 = 0$ corresponds to a lack of energy about "vertical" wavenumbers $\mathbf{k}$ (i.e., nearly aligned with the rotation axis). The contribution of these modes at "vertical" wavenumbers is to horizontal velocity or vorticity components since $\widehat{\mathbf{u}}$ and $\widehat{\boldsymbol{\omega}}$ are normal to $\mathbf{k}$. In other words, $b_{33}^{e} > 0$ (and $b_{33}^{(k^2 e)} > 0$) characterize the lessening of dimensionality in the presence of the incompressibility constraint.

4. Summary

The relevance of two threshold Rossby numbers which delineate anisotropic effects in rotating turbulence has been demonstrated using the database from high-resolution LES at asymptotically high Reynolds numbers. Anisotropy created by background rotation can only be initiated by nonlinear interactions and is triggered when a macro-Rossby number becomes smaller than 1. An excellent collapse of the main anisotropy indicators was demonstrated in terms of the macro-Rossby number.

The second transition corresponding to a micro-Rossby number Ro^ω close to 1 was found in previous experimental, EDQNM, and DNS results as the beginning of the shut-off of the energy cascade indicating that non-isotropic, non-linear effects were frozen. In the LES results used in this study, a second transition is indeed observed for $Ro^\omega < 1$ but represents a reorganization of the anisotropy rather than a stabilization. The description of this complex anisotropic structure has motivated a detailed analysis of the 'dimensionality' and 'polarization' effects of steady system rotation. These effects can be summarized by considering a rectangular domain in spectral space where $|k_3/k|$ is plotted on the vertical axis and k on the horizontal axis (Fig. 17). The domain can be separated horizontally in a narrow band $|k_3/k| < \epsilon_s << 1$ near $k_3 = 0$ (the slow manifold denoted 's') and the remaining

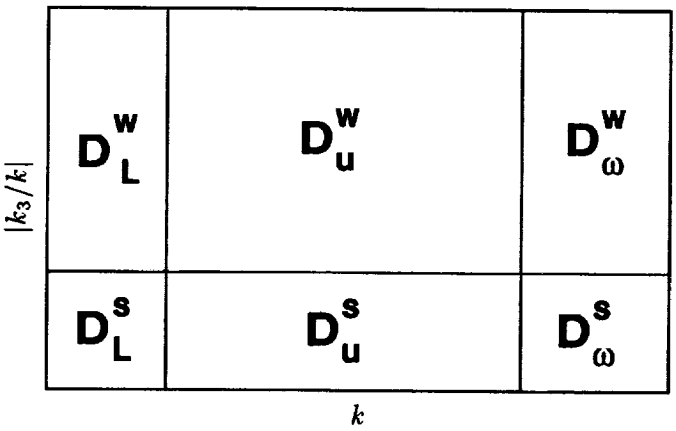

FIGURE 17. Sub-domains in k-space.

upper band (denoted 'w') where the scrambling effect of inertial waves are present. The spectral domain can be further subdivided into three bands of wavenumbers that characterize the largest scales (L), the energetic scales (u), and the vorticity scales (ω). The six sub-domains corresponding to these divisions are denoted as $D_L^w, D_u^w, D_\omega^w, D_L^s, D_u^s, D_\omega^s$ in Fig. 17. The first transition is characterized by the beginning of a lessening of dimensionality and concentration of energy towards the slow manifold in agreement with $b_{33}^e > 0$ (which characterizes an angular drain of energy from D_u^w to D_u^s) and $b^{(k^2e)} > 0$ (which characterizes an angular drain of energy from D_ω^w to D_ω^s). Polarization, or componentality, only affects the slow manifold and is reflected by $b^L > 0$ (which characterizes D_L^s). When the Rossby number is in the intermediate range ($Ro^L < 1$ and $Ro^\omega > 1$), the polarization indicators b_{33}^z and $b_{33}^{(k^2z)}$ remain weak so that the global anisotropy reflected by b_{33} and b_{33}^ω is an almost pure dimensional effect. After the second transition, the polarization effect in the slow manifold seems to emerge not only in D_L^s, but also in D_u^s through $b_{33}^z < 0$ so that $b_{33} = b_{33}^e + b_{33}^z$ results from opposite 'dimensional' and 'polarization' effects. Nevertheless, the vorticity anisotropy $b_{33}^\omega = b_{33}^{(k^2e)} - b_{33}^{(k^2z)}$ continues to be essentially due to the dimensional contribution $b_{33}^{(k^2e)}$. Such a pattern may correspond to opposite values of the polarization anisotropy in the domains D_L^s ($Z < 0 \rightarrow b^L > 0$), D_u^s ($Z < 0 \rightarrow b_{33}^z > 0$) and D_ω^s ($Z > 0$).

An analysis of the vorticity structure was performed by means of a joint-pdf representation of the $\cos\alpha = \omega_3/\omega$ and the local Rossby number $\sqrt{\omega_i\omega_i}/(2\Omega)$. The second transition ($Ro^\omega \sim 1$) is shown to be characterized by a tendency of the vortices to be aligned with the basic rotation vector with an increasing dominance of corrotative eddies. This last result could be explained by a classical Bradshaw-Richardson stability criterion (Bradshaw 1969), also consistent with Rayleigh centrifugal criterion, at least for values close to zero absolute vorticity $\omega_i + 2\Omega_i = 0$ or zero tilting vorticity $\frac{1}{2}\omega_i + 2\Omega_i$, as discussed by Cambon *et al.* (1994a). These results for the vorticity structure are also in qualitative agreement with those of Bartello *et al.* (1994). However, in the present study this is a side effect and not the main source

of the anisotropy. The fact that the maximum value of $\omega_3/(2\Omega)$ is nearly the same as Ro^ω is consistent with the fact that the componentality effect (with corresponds to a polarization effect in the slow manifold) has a relatively weak effect on the structure of the vorticity field. Statistically, the 'cigar type' shape of the vorticity correlations tensor mainly reflects the pure dimensional effect.

It should also be noted that anisotropic trends would be blocked for $Ro^\omega < 1$, except for quantities only dependent on the slow manifold (e.g., b^L), in accordance with a shut-off of the energy cascade if viscous effects were present in the simulations. The reorganization of the anisotropy (especially as reflected by b^z_{33} in the Reynolds stress as well as in the circulicity tensor) after the second transition is only allowed in the absence of dissipation.

REFERENCES

BARDINA, J., FERZIGER, J. H. & ROGALLO, R. S. 1985 Effect of rotation on isotropic turbulence: computation and modeling. *J. Fluid Mech.* **154,** 321-336.

BARTELLO, P., MÉTAIS, O. & LESIEUR, M. 1994 Coherent structures in rotating three-dimensional turbulence. *J. Fluid Mech.* **273,** 1.

BRADSHAW, P. 1969 The analogy between streamline curvature and buoyancy in turbulent shear flow. *J. Fluid Mech.* **36,** 177-191.

CAMBON, C. 1982 Étude spectrale d'un champ turbulent incompressible soumis à des effets couplés de déformation et de rotation imposés extérieurement. *Thèse de doctorat d'état, Université Claude Bernard-Lyon I.*

CAMBON, C. 1990 Single and two point modeling of homogeneous turbulence. *Annual Research Briefs,* NASA/Stanford Center for Turbulence Research, 23-38.

CAMBON, C., BERTOGLIO, J. P. & JEANDEL, D. 1981 Spectral closure of homogeneous turbulence. *AFOSR-Stanford Conf. on Complex Turb. Flows.*

CAMBON, C. & JACQUIN, L. 1989 Spectral approach to non-isotropic turbulence subjected to rotation. *J. Fluid Mech.* **202,** 295-317.

CAMBON, C., JACQUIN, L. & LUBRANO, J. L. 1992 Toward a new Reynolds stress model for rotating turbulent flows. *Phys. Fluids A.* **4,** (4), 812-824.

CAMBON C., BENOIT, J. P., SHAO, L., & JACQUIN, L. 1994a Stability analysis and large-eddy simulation of rotating turbulence with organized eddies. *J. Fluid Mech.* **278,** 1-27.

CAMBON, C., MANSOUR, N. N. & GODEFERD, F. S. 1994b The energy transfer in rotating turbulence. In preparation.

CHASNOV, J. 1994 Similarity states of passive scalar transport in isotropic turbulence. *Phys. Fluids.* **6**(2), 1036-1051.

CHOLLET, J. P. & LESIEUR, M. 1981 Parametrization of small scales of three-dimensional isotropic turbulence utilizing spectral closures.. *J. Atmos. Sci.* **38,** 2747-2757.

JACQUIN, L., LEUCHTER, O., CAMBON, C., & MATHIEU, J. 1990 Homogeneous turbulence in the presence of rotation. *J. Fluid Mech.* **220,** 1-52.

JACQUIN, L., LEUCHTER, O. & GEOFFROY, P. 1989 Experimental study of homogeneous turbulence in the presence of rotation. *6th symposium on Turbulent Shear FLows.* Springer Verlag, Heidelberg.

KRAICHNAN, R. H. 1976 Eddy viscosity in two and three dimensions. *J. Atmos. Sci.* **33,** 1521-1536.

MANSOUR, N. N., CAMBON, C. & SPEZIALE C. G. 1991a Theoretical and computational study of rotating isotropic turbulence. *Studies in Turbulence,* ed. by T. B. Gatski, S. Sarkar and C. G. Speziale, Springer Verlag, New-York.

MANSOUR, N. N., CAMBON, C. & SPEZIALE C. G. 1991b Single point modeling of initially isotropic turbulence under uniform rotation.. *Annual Research Briefs,* NASA/Stanford Center for Turbulence Research, 159-168.

MANSOUR, N. N., SHIH, T.-H. & REYNOLDS, W. C. 1991c The effects of rotation on initially anisotropic homogeneous flows. *Phys. Fluids A.* **3,** (10), 2421-2425.

PROUDMAN, J. 1916 On the motion of solids in a liquid possessing vorticity. *Proc. R. Soc. London, A.* **92,** 408.

REYNOLDS, W. C., & KASSINOS, S. 1994 A one-point model for the evolution of the Reynolds stress and structure tensors in rapidly deformed homogeneous turbulence. *Osborne Reynolds Centenary Symposium,* UMIST Manchester, United Kingdom, May 1994.

ROGALLO, R. S. 1981 Numerical experiments in homogeneous turbulence. NASA Technical Memorandum 81315.

SPEZIALE, C. G., MANSOUR, N. N., & ROGALLO, R. S. 1987 Decay of turbulence in a rapidly rotating frame. *Proc. 1987 Summer Program,* NASA/Stanford Center for Turbulence Research, Report CTR-S87, 205-212.

SQUIRES, K. D., CHASNOV, J. R., MANSOUR, N. N. & CAMBON, C. 1993 Investigation of the asymptotic state of rotating turbulence using large-eddy simulation. *Annual Research Briefs,* NASA/Stanford Center for Turbulence Research, 157-170.

SQUIRES, K. D., CHASNOV, J. R., MANSOUR, N. N. & CAMBON, C. 1994 The asymptotic state of rotating homogeneous turbulence at high Reynolds number. *AGARD Conf. Proc. CP-551,* in press.

WALEFFE, F. 1991 Non-linear interactions in homogeneous turbulence with and without background rotation. *Annual Research Briefs,* Center for Turbulence Research, NASA Ames/Stanford University, 31-43.

ZEMAN, O. 1994 A note on the spectra and decay of rotating homogeneous turbulence. To appear in *Phys. Fluids.*